Chinese Physics Letters **42**, 067405 (2025) **Express Letter**

Neutron Spin Resonance near a Lifshitz Transition in Overdoped $Ba_{0.4}K_{0.6}Fe_2As_2$

Yang Li[1,2], Dingsong Wu[1,2,3], Yingjie Shu[1,2], Bo Liu[1,2], Uwe Stuhr[4], Guochu Deng[5], Anton P. J. Stampfl[6], Lin Zhao[1,2], Xingjiang Zhou[1,2], Shiliang Li[1,2], Amit Pokhriyal[7,8], Haranath Ghosh[7,8*], Wenshan Hong[1*], and Huiqian Luo[1*]

[1]*Beijing National Laboratory for Condensed Matter Physics, Institute of Physics, Chinese Academy of Sciences, Beijing 100190, China*
[2]*School of Physical Sciences, University of Chinese Academy of Sciences, Beijing 100190, China*
[3]*Department of Physics, University of Oxford, Oxford OX1 3PU, United Kingdom*
[4]*Laboratory for Neutron Scattering and Imaging, Paul Scherrer Institute, CH-5232 Villigen PSI, Switzerland*
[5]*Australian Centre for Neutron Scattering, Australian Nuclear Science and Technology Organisation, Lucas Heights NSW 2234, Australia*
[6]*Australian Nuclear Science and Technology Organisation, Lucas Heights NSW 2234, Australia*
[7]*Theory and Computational Physics Section, Raja Ramanna Centre for Advanced Technology, Indore 452013, India*
[8]*Homi Bhabha National Institute, BARC training school complex 2nd floor, Anushakti Nagar, Mumbai 400094, India*

(Received 18 April 2025; accepted manuscript online 12 May 2025)

Elucidating the relationship between spin excitations and fermiology is essential for clarifying the pairing mechanism in iron-based superconductors (FeSCs). Here, we report inelastic neutron scattering results on the hole overdoped $Ba_{0.4}K_{0.6}Fe_2As_2$ near a Lifshitz transition, where the electron pocket at M point is nearly replaced by four hole pockets. In the normal state, the spin excitations is observed at incommensurate wave vectors with a chimney-like dispersion. By cooling down to the superconducting state, a neutron spin resonance mode emerges with a peak energy of $E_{\mathrm{r}} = 14$–$15\,\mathrm{meV}$, weakly modulated along the L-direction. The incommensurability notably increases at low energies, giving rise to downward dispersions of the resonance mode. This behavior contrasts sharply with the upward dispersions of resonance observed in optimally doped $Ba_{0.67}K_{0.33}Fe_2As_2$ contributed by the hole to electron scattering, but resembles those in KFe_2As_2 and $KCa_2Fe_4As_4F_2$ where the fermiology is dominated by hole pockets. These results highlight the critical role of electronic structure modifications near the Fermi level, especially in governing interband scattering under imperfect nesting conditions, which fundamentally shape the spin dynamics of FeSCs.

DOI: 10.1088/0256-307X/42/6/067405 CSTR: 32039.14.0256-307X.42.6.067405

Understanding the superconductivity and related phenomena in iron-based superconductors (FeSCs) is a great challenge due to their complex multiband nature.[1] Such complexity arises from multiple Fermi surfaces, diverse superconducting gap structures, intricate orbital contributions, and prominent spin fluctuations, particularly those stemming from interband scattering.[2] These factors become especially significant when comparing iron-based superconductors with different Fermi surface topologies. In most FeSCs, the Fermi surface comprises multiple hole pockets at the Γ point and hybridized electron pockets at the M point, facilitating superconductivity with $s_{\pm}$ pairing symmetry driven by spin fluctuations. These fluctuations may originate either from weak-coupling Fermi surface nesting contributed by itinerant electrons, or from strong-coupling local magnetic interactions on the Fe sites.[3–7] In contrast, systems with only electron-like Fermi pockets typically observed in electron-doped iron chalcogenides exhibit dominant d-wave pairing symmetry,[8–12] driven by inter-pocket scattering between zone corners.[13,14] The spin excitations in such systems are distinct between the parent and superconducting phases,[12,15–19] suggesting that the specific multiband Fermi surface topologies strongly influence the nature of superconductivity and quasi-particle excitations.

$Ba_{1-x}K_xFe_2As_2$ is a typical hole-doped FeSC with a broad doping range, from the parent $BaFe_2As_2$ to the fully hole doped KFe_2As_2[20–25] [Figs. 1(a) and 1(b)]. Intriguing phenomena in the overdoped region are argued to be related to a Lifshitz transition of Fermi surfaces,[26–38] where the electron pocket near the M point is replaced by four propeller-shaped hole pockets at about $x = 0.7$ [Figs. 1(c)–1(h)]. Eventually, the spin fluctuations around the perfectly nesting wavevevtor $\boldsymbol{Q}$ in the optimal doping split into two incommensurate peaks at $\boldsymbol{Q}_{1,2}$ due to the mismatch of pocket sizes [Figs. 1(f) and 1(g)].[31,39–43] Such incommensurate spin fluctuations show a strong hole doping dependence, especially in the superconducting state.[41–43] Particularly in KFe_2As_2, where only anisotropic hole pockets are present around both Γ and M points, a strongly incommensurate spin resonance mode is observed at $\boldsymbol{Q}_{1,2}$, suggesting the persistence of $s_{\pm}$ pairing symmetry [Fig. 1(h)]. Therefore, it is crucial to elucidate these fascinating behaviors by exploring the interplay between spin fluctuations and electronic structures in the overdoped regime.

*Corresponding author. Email: hng@rrcat.gov.in; wshong@iphy.ac.cn; hqluo@iphy.ac.cn

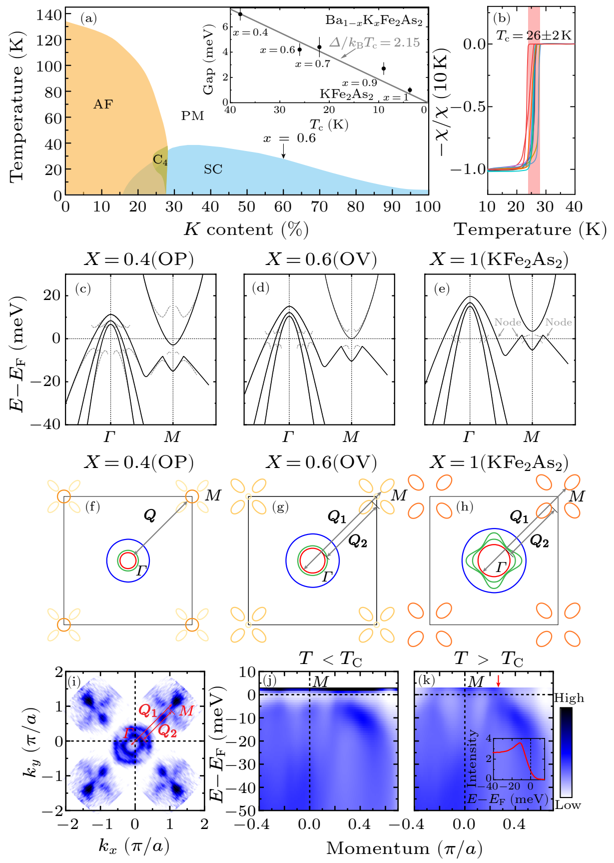

Fig. 1. Phase diagram and electronic structure of $Ba_{1-x}K_xFe_2As_2$. (a) Phase diagram of $Ba_{1-x}K_xFe_2As_2$,[20] with the arrow indicating the doping level of $x = 0.6$. The inset shows the superconducting gap size near Γ point.[21–24] (b) Zero-field-cooled magnetization measurements from multiple crystals, yielding an average T_c of 26 K. (c)–(e) Schematic representations of the band structure for $Ba_{1-x}K_xFe_2As_2$ at $x = 0.4$ (optimally doped), $x = 0.6$ (overdoped, this study), and $x = 1$ (KFe_2As_2, full overdoped). The gray dashed line marks the Bogoliubov back-bending effect due to the superconducting gap. (f)–(h) Corresponding Fermi surface illustrations, highlighting interband scattering vectors ($\boldsymbol{Q}$, $\boldsymbol{Q_1}$ and $\boldsymbol{Q_2}$). (i)–(k) ARPES measurements of the Fermi surfaces and band structure for $x = 0.6$. The inset in (k) shows the energy distribution curve at the position marked by an arrow.

In this Letter, we report the low-energy spectrum of spin excitations in the hole overdoped $Ba_{1-x}K_xFe_2As_2$ single crystals with $x = 0.6$ and $T_c = 26$ K, where the doping level is near the Lifshitz transition ($x = 0.7$) [Figs. 1(a) and 1(b)]. For $x = 0.6$ doping, the electron pocket at the M point nearly vanishes, while the propeller-shaped hole-like Fermi surfaces at the M point approach the Fermi energy (E_F), significantly altering the electronic density of states [Figs. 1(c)–1(k)]. We observe a neutron spin resonance mode at energies of 14 meV (odd L) and 15 meV (even L), exhibiting quasi-two-dimensional characteristics, with broad incommensurate peaks centered around $Q = (1, 0)$ in the magnetic unit cell [or $Q = (0.5, 0.5)$ from $(0, 0)$ to (π, π) in the nuclear unit cell, see Figs. 1(f) and 1(i)]. A comparison of the spin excitation spectra between the superconducting and normal states reveals that the excitations evolve from a nearly non-dispersive profile in the normal state to one with downward dispersion in the superconducting state, forming a clear downward dispersion of the resonance. This behavior contrasts sharply with that observed in the optimally doped $Ba_{1-x}K_xFe_2As_2$,[44–46] suggesting that in the overdoped regime, the spin fluctuations are strongly influenced by the itinerant electrons associated with the hole pockets near the M point, even though these pockets do not actually cross the Fermi level. Such modifications in Fermi surface topology drive significant changes in the physical properties of the system, especially in the spin fluctuations and electronic behaviors. Therefore, we propose a unified picture to describe the resonance dispersions which are determined by the sign-change of Fermi velocities between two nesting bands closed to the Fermi level in the superconducting state below T_c.

High-quality single crystals of overdoped $Ba_{0.4}K_{0.6}Fe_2As_2$ ($T_c = 26 \pm 2$ K) were synthesized using the self-flux method.[47,48] For neutron scattering experiments, approximately 4 grams of crystals were co-aligned on aluminum plates with hydrogen-free glue. The experiments were performed on the thermal triple-axis spectrometer EIGER at the Swiss Spallation Neutron Source, Paul Scherrer Institute, Switzerland, and the Taipan spectrometer at the Australian Centre for Neutron Scattering, ANSTO, Australia. The scattering plane $[H, 0, L]$ was defined in reciprocal lattice units (r.l.u.) as $\boldsymbol{Q} = (H, K, L) = (q_x a/2\pi, q_y b/2\pi, q_z c/2\pi)$, where the pseudo-orthorhombic magnetic unit cell parameters are $a = b = 5.2$ Å and $c = 13.22$ Å. The high-resolution angle-resolved photoemission (ARPES) measurements were carried out on our laboratory system equipped with a Scienta DA30 electron energy analyzer. We use a helium I resonance line as the light source which provides a photon energy of $h\nu = 21.218$ eV. The energy resolution was set to 10 meV and the angular resolution to 0.3°. As shown in Figs. 1(i)–1(k), the ARPES results clearly demonstrate the fermiology and band structure similar to the calculated results using density functional theory (DFT) with the plane wave basis set approach implemented in Quantum ESPRESSO package [Figs. 1(d) and 1(g)].[49,50] The superconducting gap on the hole pockets around Γ point follows a linear relation with T_c ($\Delta/k_BT_c = 2.15$) along with other dopings in $Ba_{1-x}K_xFe_2As_2$.[21–24]

Figure 2 presents the results of neutron spin resonance mode in $Ba_{0.4}K_{0.6}Fe_2As_2$. Figures 2(a) and 2(b) show the raw data collected below and above T_c for odd and even L values, respectively. The choice of L values is critical for extracting mode energy and intensity, which can be estimated from the magnetic interaction associated with the distance between the FeAs layers.[51–53] In $Ba_{0.4}K_{0.6}Fe_2As_2$, the difference in mode energy and intensity between odd and even L values is minimal, as illustrated in Fig. 2(c). The mode energy is 14 meV for odd L values and 15 meV for even L values at the incommensurate wave vector $(1.18, 0, L)$, with maximum intensity depletion occurring around 7 meV. Given the small discrepancy in the resonance modes between $L = 2$ and $L = 3$, we selected $L = 3$ for further investigation. Notably, the mode energy remains identical to that of optimally doped $Ba_{1-x}K_xFe_2As_2$,[44–46] which peaks at a commensurate H position, despite a 30% reduction in T_c.

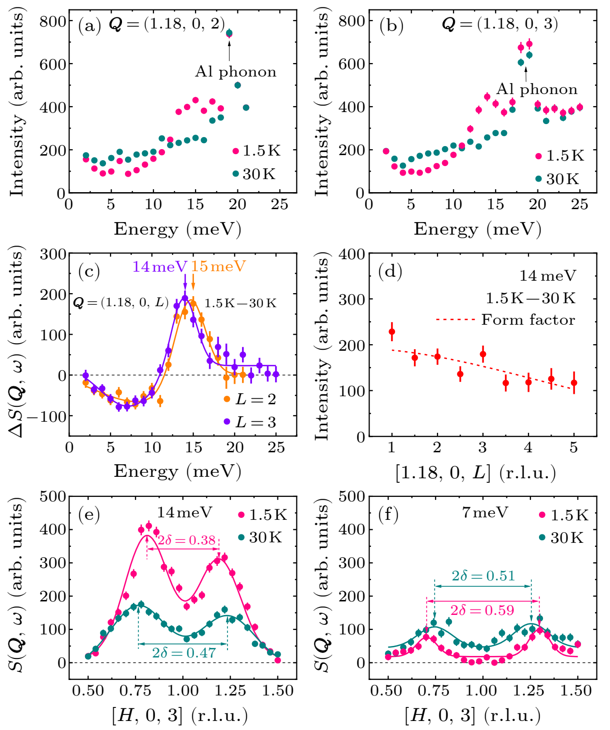

Fig. 2. Neutron spin resonance in $Ba_{0.4}K_{0.6}Fe_2As_2$. (a) and (b) Energy scans at two incommensurate wave vectors: $\boldsymbol{Q}$ = (1.18, 0, 2) and (1.18, 0, 3), measured below and above T_c. Anomalous data points originate from aluminum phonon contributions. (c) Temperature difference plot based on the data in (a) and (b), with arrows marking the resonance energies at $\boldsymbol{Q}$ = (1.18, 0, 2) (15 meV) and $\boldsymbol{Q}$ = (1.18, 0, 3) (14 meV). (d) L-modulation of the resonance, where the dashed line represents the square of the magnetic form factor of Fe^{2+} after normalizing to the intensity. (e) and (f) Constant-energy scans at E = 14 meV and 7 meV along the (H, 0, 3) direction, taken below and above T_c. Solid lines represent two-peak Gaussian fits to the data with the incommensurability δ.

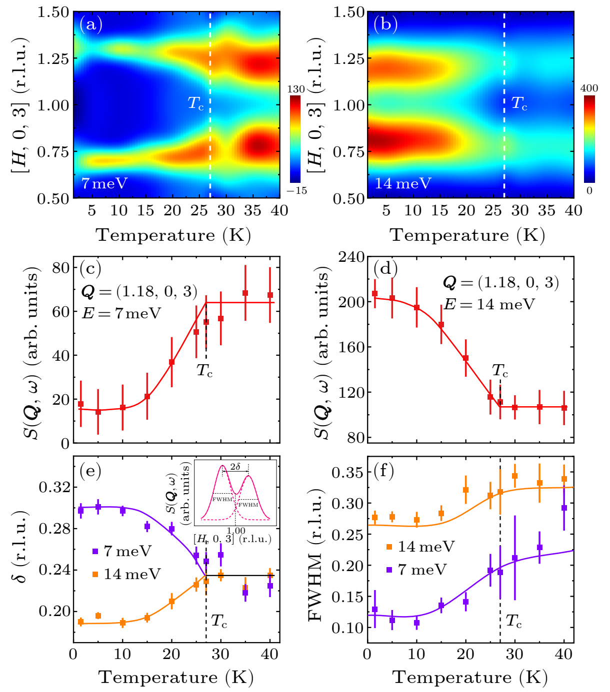

Fig. 3. Temperature dependence of spin excitations in $Ba_{0.4}K_{0.6}Fe_2As_2$. (a) and (b) Spin excitations along the (H, 0, 3) direction at E = 7 meV and 14 meV, respectively. (c) and (d) Temperature dependence of spin excitations at fixed $\boldsymbol{Q}$ = (1.18, 0, 3) with E = 7 meV and 14 meV. (e) and (f) Extracted incommensurability (δ) and full width at half maximum (FWHM) as a function of temperature for energy transfers of 7 meV and 14 meV. Solid lines in (c)–(f) are guides to the eyes. The definition of δ and FWHM are illustrated in the inset of (e).

The L-modulation of the resonance follows the square of the magnetic form factor of Fe^{2+}, as shown in Fig. 2(d), confirming its magnetic origin. The selection of incommensurate positions, essential for determining the resonance energy, is based on a combination of energy and $\boldsymbol{Q}$ scans, where the resonance signal is maximized, as shown in Fig. 2(e). Figures 2(e) and 2(f) present typical energy and momentum scans below and above T_c. For the resonance energy E = 14 meV, the incommensurability decreases in the superconducting state, while for E = 7 meV in the depletion region, it increases. This behavior can be attributed to the opening of superconducting gaps, which affects the distribution of pairing electrons near E_F [Figs. 1(j) and 1(k)].

To explore the effects of superconductivity on low-energy spin excitations, we have performed temperature-dependent measurements at the wave vector (1.18, 0, 3) with energy transfers of 7 meV and 14 meV, as illustrated in Fig. 3. The results, displayed in Figs. 3(a) and 3(b), reveal a significant suppression of intensity at 7 meV in the superconducting state. This suppression can be attributed to the redistribution of spectral weight caused by the opening of the superconducting gap, which shifts the density of states to higher energies, as evidenced by the enhanced intensity at 14 meV. The dynamic structure factor $S(\boldsymbol{Q},\omega)$ shows temperature dependence resembling an order parameter [Figs. 3(c) and 3(d)], reinforcing the connection between the observed spin excitations and superconductivity. The different temperature evolution of the incommensurability below T_c, shown in Fig. 3(e), possibly originates from the redistribution of electronic states in the momentum space, likely reflecting changes in interband scattering processes. The peak width narrowing at both energies in the superconducting state [Fig. 3(f)] suggests enhanced localization of magnetic scattering, consistent with the condensation of Cooper pairs.

To investigate the impact of electronic structure changes near the M point on the dispersion of spin excitations in $Ba_{0.4}K_{0.6}Fe_2As_2$, we have also performed $\boldsymbol{Q}$-scans from E = 5 to 19 meV. The corresponding results, shown in Fig. 4, are compared with those from optimally doped $Ba_{0.67}K_{0.33}Fe_2As_2$ and fully overdoped KFe_2As_2.[16,31,32,45,46] Figures 4(a) and 4(b) present low-energy spin fluctuations below and above T_c. The incommensurability (δ) at various energies, determined by fitting with a two-peak Gaussian function, is summarized in Figs. 4(d) and 4(e). The net intensity and dispersion of resonance are shown in Figs. 4(c) and 4(f).

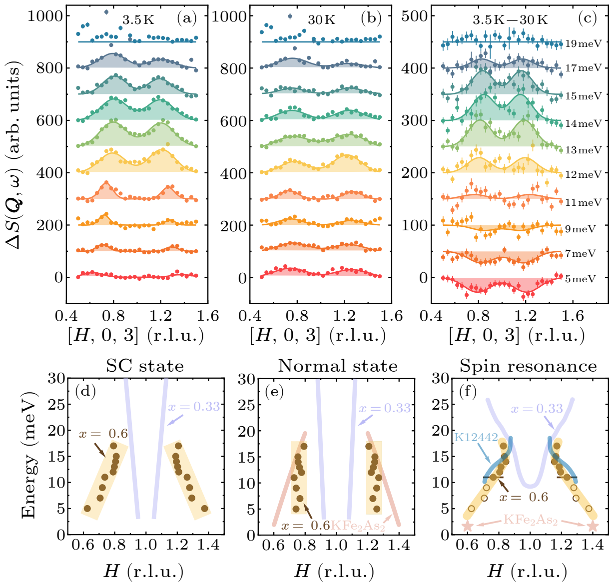

Fig. 4. Low-energy spin excitations in $Ba_{1-x}K_xFe_2As_2$. (a) and (b) Low-energy spin excitations in $Ba_{0.4}K_{0.6}Fe_2As_2$ along the $(H,\ 0,\ 3)$ direction in both the normal and superconducting states from 5 meV to 19 meV. Solid lines represent two-peak Gaussian fits to the data, and the shaded area highlights the spin excitation signal. (c) Temperature difference plots of low-energy excitations. (d) and (e) Comparison of low-energy spin excitations in $Ba_{1-x}K_xFe_2As_2$ [$x = 0.33$, 1 and from this work, 0.6, extracted from the fits in (a) and (b)] in the normal and superconducting states along the in-plane H direction.[16,31,32,46] (f) Comparison of resonance dispersion in $Ba_{1-x}K_xFe_2As_2$ ($x = 0.33$, 0.6 and 1) and $KCa_2Fe_4As_4F_2$ (K12442), with open circles for $x = 0.6$ representing negative net intensity.

In $Ba_{0.4}K_{0.6}Fe_2As_2$, the normal-state spin excitations at the incommensurate wave vectors exhibit minimal dispersion. Upon entering the superconducting state, these excitations develop a downward-dispersive behavior. This contrasts sharply with the optimally doped $Ba_{0.67}K_{0.33}Fe_2As_2$, where the spin fluctuations are centered at the commensurate vector $\boldsymbol{Q} = (1,\ 0)$ and exhibit upward dispersion both below and above T_c [Figs. 4(d) and 4(e)].[16,45,46] The modification in low-energy fluctuations in $Ba_{0.4}K_{0.6}Fe_2As_2$ may be driven by the Lifshitz transition at the M point. This interpretation is further supported by the large incommensurability observed in KFe_2As_2 due to the strongly imperfect nesting between hole pockets near the $\varGamma$ and M points [Fig. 1(h)].[21,32,43] Notably, the resonance energy (E_r) in the $x = 0.6$ compound is the same as $x = 0.33$, resulting in $E_r/k_BT_c \approx 6.7$. This deviates from the typical $E_r/k_BT_c \approx 4.9$ observed in other FeSCs but close to the $E_r/k_BT_c \approx 5.8$ in cuprates,[54,55] which could be a consequence of the strong-coupling Cooper pairs in hole-overdoped compounds similar to the case in $KCa_2Fe_4As_4F_2$ ($\varDelta_{tot}/k_BT_c \approx 6$)[45,46,56–58]. Here the estimated $\varDelta_{tot}/k_BT_c \approx 9$ for $Ba_{0.4}K_{0.6}Fe_2As_2$ ($\varDelta_{tot} \approx 10.3$ meV), by supposing the proportional relation between gap and T_c [inset of Fig. 1(a)].[46] Moreover, both the E_r over than $2\varDelta$ and the downward dispersion of resonance recall the case in $KCa_2Fe_4As_4F_2$ (K12442) [Fig. 4(f)], which defy explanation by the conventional spin-exciton scenario under the $s^{\pm}$-pairing.[56,59,60]

It is intriguing to correlate the Fermi surface topologies with low-energy spin excitations in the overdoped $Ba_{1-x}K_xFe_2As_2$. The downward dispersion of resonance may be due to the approach of hole pockets near E_F at M point, since the gap opening will expose the hole bands below E_F but push away the electron bands above E_F [dashed lines in Figs. 1(c) and 1(e)]. As the hole concentration increases further to $x = 1$ (namely KFe_2As_2), the Fermi surfaces near the M point are dominated by four propeller-like hole pockets.[21,22] Although the superconducting gaps become nodal-like in these hole pockets, the pairing symmetry is still of the $s^{\pm}$-type.[21,32,43] In this case, the downward dispersion of resonance could be a consequence of size-mismatched hole to hole scattering, where the Fermi velocity (V_F) does not change sign between two nesting bands. In those optimally hole or electron doped compounds, the resonance mode is contributed by the scattering between hole and electron bands, thus its dispersion should be upward due to the sign change of V_F.[45,46,56] Interestingly, such simple picture can be also applied to those iron chalcogenides with only electron pockets, where the spin excitations show an hour-glass type of dispersion in the superconducting state similar to the hole-type cuprates.[12,61] Therefore, we can establish a universal picture of the resonance dispersion in FeSCs, it is solely determined by the sign-change of Fermi velocities between two nesting bands after gap opening below T_c. This means the resonance dispersion does not have to follow the gap distribution in the momentum space, but it is intimately connected to the band structure near E_F. In most cases E_r could be related to $\varDelta$ and T_c, but not always follow the linear scaling law when the interband scattering changes below T_c.[1,12,61]

To conclude, we used inelastic neutron scattering to investigate the low-energy spin excitations in the overdoped $Ba_{0.4}K_{0.6}Fe_2As_2$ near a Lifshitz transition. We identified a spin resonance mode with a peak energy E_r similar to that found in optimally doped $Ba_{0.67}K_{0.33}Fe_2As_2$, despite a significantly reduced T_c. In contrast to the commensurate resonance mode and upward in-plane dispersion observed at the optimal doping, the resonance in the overdoped sample emerges at incommensurate wave vectors and exhibits a pronounced downward dispersion. These results challenge the prevailing view of the resonance as a magnetic exciton confined by the superconducting gaps, suggesting that its properties are strongly influenced by the changes in the Fermi surface topology. By establishing a unified picture of the resonance dispersions determined by the sign-change of Fermi velocities, our results underscore the pivotal role of Fermi surface evolution in driving the spin dynamics and electronic structure of FeSCs. Further experimental and theoretical work is essential to disentangle the complex interplay between multiband scattering and unconventional superconductivity, offering new insights into the roles of these low-energy collective excitations in the superconducting pairing mechanism.

Acknowledgements. This work is supported by the National Key Research and Development Program of China (Grant Nos. 2023YFA1406100, 2018YFA0704200, 2022YFA1403400 and 2021YFA1400400), the National Natural Science Foundation of China (Grant Nos. 11822411 and 12274444), the Strategic Priority Research Program (B) of the CAS (Grant Nos. XDB25000000 and XDB33000000) and K. C. Wong Education Foundation (GJTD-2020-01). AP and HG acknowledge the Computer Division at RRCAT for providing the scientific computing facilities. Financial support for this study was provided to AP by HBNI-RRCAT and MPCST under the FTYS program. This work is based on neutron scattering experiments performed at the Swiss Spallation Neutron Source (SINQ), Paul Scherrer Institute, Villigen, Switzerland (Proposal No. 20212794), and the Australian Centre for Neutron Scattering (ACNS), Australian Nuclear Science and Technology Organisation, Australia (Proposal Nos. P9850 and P9882).

References

[1] Scalapino D J 2012 *Rev. Mod. Phys.* **84** 1383

[2] Fernandes R M, Coldea A I, Ding H, Fisher I R, Hirschfeld P J, and Kotliar G 2022 *Nature* **601** 35

[3] Mazin I I, Singh D J, Johannes M D, and Du M H 2008 *Phys. Rev. Lett.* **101** 057003

[4] Kuroki K, Onari S, Arita R, Usui H, Tanaka Y, Kontani H, and Aoki H 2008 *Phys. Rev. Lett.* **101** 087004

[5] Si Q and Abrahams E 2008 *Phys. Rev. Lett.* **101** 076401

[6] Seo K, Bernevig B A, and Hu J 2008 *Phys. Rev. Lett.* **101** 206404

[7] Dai P 2015 *Rev. Mod. Phys.* **87** 855

[8] Zhang Y, Yang L X, Xu M, Ye Z R, Chen F, He C, Xu H C, Jiang J, Xie B P, Ying J J *et al.* 2011 *Nat. Mater.* **10** 273

[9] Qian T, Wang X P, Jin W C, Zhang P, Richard P, Xu G, Dai X, Fang Z, Guo J G, Chen X L, and Ding H 2011 *Phys. Rev. Lett.* **106** 187001

[10] Liu D F, Zhang W H, Mou D X, He J F, Ou Y B, Wang Q Y, Li Z, Wang L L, Zhao L, He S L, Peng Y Y, Liu X, Chen C Y, Yu L, Liu G D, Dong X L, Zhang J, Chen C T, Xu Z Y, Hu J P, Chen X, Ma X C, Xue Q K, and Zhou X J 2012 *Nat. Commun.* **3** 931

[11] Zhao L, Liang A, Yuan D, Hu Y, Liu D, Huang J, He S, Shen B, Xu Y, Liu X, Yu L, Liu G, Zhou H, Huang Y, Dong X, Zhou F, Liu K, Lu Z, Zhao Z, Chen C, Xu Z, and Zhou X J 2016 *Nat. Commun.* **7** 10608

[12] Wo H, Pan B, Hu D, Feng Y, Christianson A D, and Zhao J 2025 *Phys. Rev. Lett.* **134** 016501

[13] Maier T A, Graser S, Hirschfeld P J, and Scalapino D J 2011 *Phys. Rev. B* **83** 100515

[14] Wang F, Yang F, Gao M, Lu Z Y, Xiang T, and Lee D H 2011 *Europhys. Lett.* **93** 57003

[15] Dai P, Hu J, and Dagotto E 2012 *Nat. Phys.* **8** 709

[16] Wang M, Zhang C, Lu X, Tan G, Luo H, Song Y, Wang M, Zhang X, Goremychkin E A, Perring T G, Maier T A, Yin Z, Haule K, Kotliar G, and Dai P 2013 *Nat. Commun.* **4** 2874

[17] Pan B, Shen Y, Hu D *et al.* 2017 *Nat. Commun.* **8** 123

[18] Friemel G, Park J T, Maier T A, Tsurkan V, Li Y, Deisenhofer J, Krug von Nidda H A, Loidl A, Ivanov A, Keimer B, and Inosov D S 2012 *Phys. Rev. B* **85** 140511

[19] Wang M, Li C, Abernathy D L, Song Y, Carr S V, Lu X, Li S, Yamani Z, Hu J, Xiang T, and Dai P 2012 *Phys. Rev. B* **86** 024502

[20] Böhmer A E, Hardy F, Wang L, Wolf T, Schweiss P, and Meingast C 2015 *Nat. Commun.* **6** 7911

[21] Wu D, Jia J, Yang J, Hong W, Shu Y, Miao T, Yan H, Rong H, Ai P, Zhang X, Yin C, Liu J, Chen H, Yang Y, Peng C, Li C, Zhang S, Zhang F, Yang F, Wang Z, Zong N, Liu L, Li R, Wang X, Peng Q, Mao H, Liu G, Li S, Chen Y, Luo H, Wu X, Xu Z, Zhao L, and Zhou X J 2024 *Nat. Phys.* **20** 571

[22] Xu N, Richard P, Shi X, van Roekeghem A, Qian T, Razzoli E, Rienks E, Chen G F, Ieki E, Nakayama K, Sato T, Takahashi T, Shi M, and Ding H 2013 *Phys. Rev. B* **88** 220508

[23] Nakayama K, Sato T, Richard P, Xu Y M, Kawahara T, Umezawa K, Qian T, Neupane M, Chen G F, Ding H, and Takahashi T 2011 *Phys. Rev. B* **83** 020501

[24] Cai Y Q, Huang J W, Miao T M, Wu D S, Gao Q, Li C, Xu Y, Jia J J, Wang Q Y, Huang Y, Liu G D, Zhang F F, Zhang S J, Yang F, Wang Z M, Peng Q J, Xu Z Y, Zhao L, and Zhou X J 2021 *Sci. Bull.* **66** 1839

[25] Kihou K, Saito T, Fujita K, Ishida S, Nakajima M, Horigane K, Fukazawa H, Kohori Y, Uchida S I, Akimitsu J, Iyo A, Lee C H, and Eisaki H 2016 *J. Phys. Soc. Jpn.* **85** 034718

[26] Thomale R, Platt C, Hanke W, Hu J, and Bernevig B A 2011 *Phys. Rev. Lett.* **107** 117001

[27] Grinenko V, Sarkar R, Kihou K, Lee C H, Morozov I, Aswartham S, Büchner B, Chekhonin P, Skrotzki W, Nenkov K, Hühne R, Nielsch K, Drechsler S L, Vadimov V L, Silaev M A, Volkov P A, Eremin I, Luetkens H, and Klauss H H 2020 *Nat. Phys.* **16** 789

[28] Bärtl F, Stegani N, Caglieris F, Shipulin I, Li Y, Hu Q, Zheng Y, Yim C, Luther S, Wosnitza J *et al.* 2025 arXiv:2501.11936 [cond-mat.supr-con]

[29] Iguchi Y, Shi R A, Kihou K, Lee C H, Barkman M, Benfenati A L, Grinenko V, Babaev E, and Moler K A 2023 *Science* **380** 1244

[30] Hu Q, Zheng Y, Xu H, Deng J, Liang C, Yang F, Wang Z, Grinenko V, Lv B, Ding H, and Yim C M 2025 *Nat. Commun.* **16** 253

[31] Lee C H, Kihou K, Kawano-Furukawa H, Saito T, Iyo A, Eisaki H, Fukazawa H, Kohori Y, Suzuki K, Usui H, Kuroki K, and Yamada K 2011 *Phys. Rev. Lett.* **106** 067003

[32] Shen S, Zhang X, Wo H, Shen Y, Feng Y, Schneidewind A, Čermák P, Wang W, and Zhao J 2020 *Phys. Rev. Lett.* **124** 017001

[33] Malaeb W, Shimojima T, Ishida Y, Okazaki K, Ota Y, Ohgushi K, Kihou K, Saito T, Lee C H, Ishida S, Nakajima M, Uchida S, Fukazawa H, Kohori Y, Iyo A, Eisaki H, Chen C T, Watanabe S, Ikeda H, and Shin S 2012 *Phys. Rev. B* **86** 165117

[34] Grinenko V, Materne P, Sarkar R, Luetkens H, Kihou K, Lee C H, Akhmadaliev S, Efremov D V, Drechsler S L, and Klauss H H 2017 *Phys. Rev. B* **95** 214511

[35] Terashima T, Kimata M, Kurita N, Satsukawa H, Harada A, Hazama K, Imai M, Sato A, Kihou K, Lee C H, Kito H, Eisaki H, Iyo A, Saito T, Fukazawa H, Kohori Y, Harima H, and Uji S 2010 *J. Phys. Soc. Jpn.* **79** 053702

[36] Terashima T, Kurita N, Kimata M, Tomita M, Tsuchiya S, Imai M, Sato A, Kihou K, Lee C H, Kito H, Eisaki H, Iyo A, Saito T, Fukazawa H, Kohori Y, Harima H, and Uji S 2013 *Phys. Rev. B* **87** 224512

[37] Hardy F, Böhmer A E, Aoki D, Burger P, Wolf T, Schweiss P, Heid R, Adelmann P, Yao Y X, Kotliar G, Schmalian J, and Meingast C 2013 *Phys. Rev. Lett.* **111** 027002

[38] Hardy F, Böhmer A E, de' Medici L, Capone M, Giovannetti G, Eder R, Wang L, He M, Wolf T, Schweiss P, Heid R, Herbig A, Adelmann P, Fisher R A, and Meingast C 2016 *Phys. Rev. B* **94** 205113

[39] Ding H, Richard P, Nakayama K, Sugawara K, Arakane T, Sekiba Y, Takayama A, Souma S, Sato T, Takahashi T, Wang Z, Dai X, Fang Z, Chen G F, Luo J L, and Wang N L 2008 *Europhys. Lett.* **83** 47001

[40] Okazaki K, Ota Y, Kotani Y, Malaeb W, Ishida Y, Shimojima T, Kiss T, Watanabe S, Chen C T, Kihou K, Lee C H, Iyo A, Eisaki H, Saito T, Fukazawa H, Kohori Y,

Hashimoto K, Shibauchi T, Matsuda Y, Ikeda H, Miyahara H, Arita R, Chainani A, and Shin S 2012 *Science* **337** 1314

[41] Castellan J P, Rosenkranz S, Goremychkin E A, Chung D Y, Todorov I S, Kanatzidis M G, Eremin I, Knolle J, Chubukov A V, Maiti S, Norman M R, Weber F, Claus H, Guidi T, Bewley R I, and Osborn R 2011 *Phys. Rev. Lett.* **107** 177003

[42] Horigane K, Kihou K, Fujita K, Kajimoto R, Ikeuchi K, Ji S, Akimitsu J, and Lee C H 2016 *Sci. Rep.* **6** 33303

[43] Lee C H, Kihou K, Park J T, Horigane K, Fujita K, Waßer F, Qureshi N, Sidis Y, Akimitsu J, and Braden M 2016 *Sci. Rep.* **6** 23424

[44] Zhang C L, Wang M, Luo H Q, Wang M Y, Liu M S, Zhao J, Abernathy D L, Maier T A, Marty K, Lumsden M D, Chi S X, Chang S, Rodriguez-Rivera J A, Lynn J W, Xiang T, Hu J P, and Dai P C 2011 *Sci. Rep.* **1** 115

[45] Zhang R, Wang W, Maier T A, Wang M, Stone M B, Chi S, Winn B, and Dai P 2018 *Phys. Rev. B* **98** 060502

[46] Xie T, Liu C, Fennell T, Stuhr U, Li S L, and Luo H Q 2021 *Chin. Phys. B* **30** 127402

[47] Luo H Q, Wang Z S, Yang H, Cheng P, Zhu X Y, and Wen H H 2008 *Supercond. Sci. Technol.* **21** 125014

[48] Luo H Q, Cheng P, Wang Z S, Yang H, Jia Y, Fang L, Ren C, Shan L, and Wen H H 2009 *Physica C* **469** 477

[49] Giannozzi P, Andreussi O, Brumme T, Bunau O, Nardelli M B, Calandra M, Car R, Cavazzoni C, Ceresoli D, Cococcioni M *et al.* 2017 *J. Phys.: Condens. Matter* **29** 465901

[50] Perdew J P, Burke K, and Ernzerhof M 1996 *Phys. Rev. Lett.* **77** 3865

[51] Lee C H, Steffens P, Qureshi N, Nakajima M, Kihou K, Iyo A, Eisaki H, and Braden M 2013 *Phys. Rev. Lett.* **111** 167002

[52] Waßer F, Park J T, Aswartham S, Wurmehl S, Sidis Y, Steffens P, Schmalzl K, Büchner B, and Braden M 2019 *npj Quantum Mater.* **4** 59

[53] Hong W, Zhou H, Li Z, Li Y, Stuhr U, Pokhriyal A, Ghosh H, Tao Z, Lu X, Hu J, Li S, and Luo H 2023 *Phys. Rev. B* **107** 224514

[54] Xie T, Gong D L, Ghosh H, Ghosh A, Soda M, Masuda T, Itoh S, Bourdarot F, Regnault L P, Danilkin S, Li S L, and Luo H Q 2018 *Phys. Rev. Lett.* **120** 137001

[55] Eschrig M 2006 *Adv. Phys.* **55** 47

[56] Kim M G, Tucker G S, Pratt D K, Ran S, Thaler A, Christianson A D, Marty K, Calder S, Podlesnyak A, Bud'ko S L, Canfield P C, Kreyssig A, Goldman A I, and McQueeney R J 2013 *Phys. Rev. Lett.* **110** 177002

[57] Hong W, Song L, Liu B, Li Z, Zeng Z, Li Y, Wu D, Sui Q, Xie T, Danilkin S, Ghosh H, Ghosh A, Hu J, Zhao L, Zhou X, Qiu X, Li S, and Luo H 2020 *Phys. Rev. Lett.* **125** 117002

[58] Fujita M, Hiraka H, Matsuda M, Matsuura M, Tranquada J M, Wakimoto S, Xu G, and Yamada K 2012 *J. Phys. Soc. Jpn.* **81** 011007

[59] Maier T A, Graser S, Scalapino D J, and Hirschfeld P 2009 *Phys. Rev. B* **79** 134520

[60] Das T and Balatsky A V 2011 *Phys. Rev. Lett.* **106** 157004

[61] Sidis Y, Pailhès S, Hinkov V, Fauqué B, Ulrich C, Capogna L, Ivanov A, Regnault L P, Keimer B, and Bourges P 2007 *C. R. Phys.* **8** 745